**Atmospheric
Chemistry
and Physics**

On the origin of tropospheric O_3 over the Indian Ocean during the winter monsoon: African biomass burning vs. stratosphere-troposphere exchange

A. T. J. de Laat

Space Research Organization Netherlands (SRON), The Netherlands

Abstract. This study investigates the origin of a commonly observed feature in the O_3 profiles: mid tropospheric O_3 maxima (300–500 hPa) over the tropical Indian Ocean. A comparison and analysis of model simulations, using a 3-D global climate-chemistry model, and measured O_3 profiles from the INDOEX campaign is presented. European Centre for Medium-Range Weather Forecast (ECMWF) meteorological analyses have been assimilated into the 3-D model to represent actual meteorology. The model realistically simulates the observed mid-tropospheric O_3 maxima. The analysis of the model simulations shows that the major source of the mid-tropospheric O_3 maxima is advection of polluted air masses from continental biomass burning areas over Africa, with generally only a small contribution of stratospheric O_3. Previous studies hinted at stratosphere-troposphere exchange (STE) along the subtropical jet (STJ) as the primary source of the mid-tropospheric O_3 maxima over the Indian Ocean. Analysis of the model simulations shows that the mechanism causing the mid-tropospheric transport of African biomass burning pollution and stratospheric air masses are frontal zones or waves passing along the subtropical jets, causing advection of tropical air masses in the prefrontal (equatorward) zone. Furthermore, the frontal zones or waves also cause STE at the poleward side of the STJ. The model simulations also indicate that the contribution of STE in general is minor compared to advection and in situ tropospheric production of O_3 for the mid-tropospheric O_3 budget over the Indian Ocean region.

1 Introduction

The INDian Ocean Experiment (INDOEX) has provided invaluable observations about the chemical composition of the Indian Ocean atmosphere, in particular O_3, during the winter

Correspondence to: A. T. J. de Laat (a.t.j.de.laat@sron.nl)

monsoon period (typical November–April). The INDOEX measurements show the presence of free-tropospheric layers with enhanced O_3 mixing ratios (de Laat et al., 1999; Mandal et al., 1999; Zachariasse et al., 2000; Peshin et al., 2001; Zachariasse et al., 2001). These layers can be found throughout the free troposphere. Generally, a typical O_3 profile over the Indian Ocean can be divided into several layers. In the marine boundary layer O_3 mixing ratios are low (outside of coastal regions), caused by an O_3-destructive environment (Rhoads et al., 1997; Lal et al., 1998; de Laat and Lelieveld, 2000; Lawrence and Lal, 2001). Between the boundary layer and 8 km O_3 mixing ratios are higher. Between 8 and 12 to 14 km is the zone where convective outflow occurs. This layer can be either high or low in O_3, depending on the origin of the air masses that were transported by the convection to this altitude. Finally, an upper-tropospheric layer may be found between 12 to 14 km and the tropopause (typically 17 km over the tropical Indian Ocean). In this layer O_3 mixing ratios are generally high, although on occasion the layer of convective outflow may extend up to the tropopause.

The upper-tropospheric layers with enhanced O_3 mixing ratios are also reported by Folkins et al. (1999), in O_3 profiles measured at Samoa (14 S, 170 W) in the Pacific Ocean. Based on the $O_3 - \theta_e$ (equivalent potential temperature) correlation they concluded that air masses below 14 km altitude generally were of tropospheric origin, whereas above 14 km the correlation suggested a stratospheric origin. Furthermore, Folkins et al. (1999) used temperature and humidity profiles to show that convection generally cannot reach altitudes above 14 km over tropical oceans.

Zachariasse et al. (2000) reported similar upper-tropospheric layers with enhanced O_3 during the First Field Phase (FFP) of INDOEX, which took place during February and March 1998. They used trajectory analysis and potential vorticity fields derived from the European Center for Medium-Range Weather Forecast (ECMWF) to conclude that STE along the northern hemispheric subtropical jet (NH-
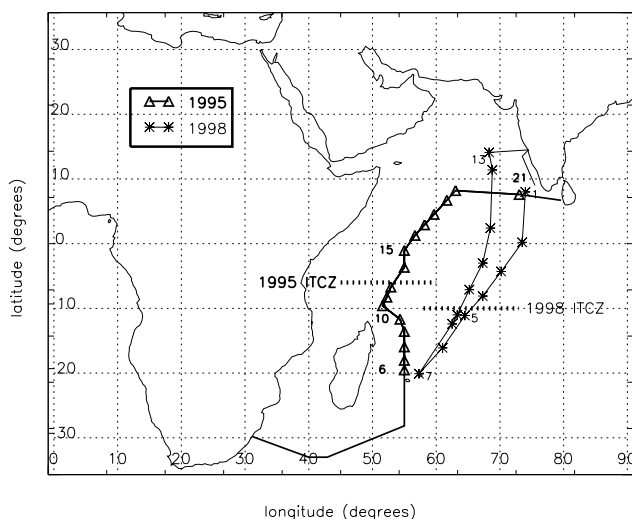
Fig. 1. Ship tracks of the 1995 (R/V Malcolm Baldrige) and 1998 (R/V Sagar Kanya) INDOEX cruises. The locations of the ozone sonde launches as summarized in tables 1 and 2 are also indicated.

STJ) was the major source of the upper-tropospheric O_3 laminae, either by shear-induced differential advection or clear-air turbulence.

The mid-tropospheric O_3 maxima are often associated with (very) low relative humidity (Peshin et al., 2001; Zachariasse et al., 2001). Zachariasse et al. (2001) used this as an indication that the polluted boundary layer over the northern Indian Ocean and India could not be the source of the mid-tropospheric O_3 maxima. They also noted that mid-tropospheric air masses might travel deep into the tropics. de Laat et al. (1999) reported similar mid-tropospheric O_3 maxima, observed during March and April 1995. However, these measurements were made closer to Africa (see Fig. 1) and also close to the ITCZ. A 3-D model analysis as well as back-trajectory calculations showed that the major source of these maxima was biomass burning over Africa, with a possible contribution from STE along the southern hemispheric sub-tropical jet (SH-STJ). Enhanced mid-tropospheric O_3 mixing ratios were also observed in O_3 profiles measured at Réunion Island during the same period (Baray et al., 1999). Their trajectory and potential vorticity analysis indicated that STE due to the interaction of tropical cyclone Marlene with the SH-STJ could give rise to the O_3 maxima they measured. Baray et al. (2001) noted in a comment on de Laat et al. (1999) that some profiles from both de Laat et al. (1999) and Baray et al. (1999) might have the same source regions since they were measured at close locations and at approximately the same time. They questioned whether biomass burning really could be the source because the biomass burning season in Africa south of the equator ends in December. However, in a subsequent reply de Laat and Lelieveld (2001) used 3-D global chemistry-climate model simulations to show that STE was not the source of the O_3 maxima. Fur-

thermore, they also noted that the modeled O_3 maxima were associated with high CO peaks, another indication that the source of the O_3 maxima was tropospheric. In a case study of an extreme pollution event over Réunion Island (Randriambelo et al., 1999) the authors noted there is a need for more thorough model analyses of the chemical and dynamical processes taking place over the southern Indian Ocean region.

More recently, a study by de Laat et al. (2001) investigated the tropospheric source regions of Carbon Monoxide (CO) over the Indian Ocean. Some indications were found of a contribution of African biomass burning to free-tropospheric air masses over the northern Indian Ocean.

2   Model description

The general circulation model (GCM) used for this study is the 19-layer European Center HAMburg Model (ECHAM), version 4. Model simulations were performed at T30-resolution, approximately $3.75° \times 3.75°$ with a time resolution of 1800 s. The model uses a hybrid $\sigma - \rho$ vertical coordinate system from the surface to 10 hPa. Average pressure levels are 990, 970, 950, 900, 840, 760, 670, 580, 490, 400, 320, 250, 190, 140, 100, 70, 50, 30 and 10 hPa. Corresponding approximate midlayer altitudes are 0.03, 0.14, 0.38, 0.78, 1.4, 2.1, 3.1, 4.2, 5.6, 7.0, 8.6, 10.2, 11.9, 13.8, 15.9, 18.0, 20.5, 23.8 and 31 km. Tracer transport is calculated using a semi-Lagrangian advection scheme (Rasch and Williamson, 1990). Vertical transport is included through parameterizations of vertical diffusion (Roeckner et al., 1996) and convection (Tiedtke, 1989). A detailed description of ECHAM version 4 is given by Roeckner et al. (1996), Haskins et al. (1995), and Chen and Roeckner (1996).

For this study, I used the standard background chemistry scheme which includes $CH_4 - CO - NO_X - HO_X$ chemistry, emissions of NO and CO, dry deposition of O_3, NO_x, HNO_3 and H_2O_2, and wet deposition of HNO_3 and H_2O_2. Concentration changes due to chemical reactions are calculated explicitly for all species by means of an Eulerian Backward Iterative (EBI) scheme (Hertel et al., 1993). A detailed description of the coupled chemistry GCM is given by Roelofs and Lelieveld (1995, 1997).

The model considers a biomass burning source of 6 Tg N yr^{-1} for NO and of 700 Tg CO yr^{-1} for CO, geographically and seasonally distributed according to Hao and Liu (1994). NO emissions from soils, 5.5 Tg N yr^{-1}, are distributed geographically and seasonally according to Yienger and Levy (1995). Lightning NO_X emissions, 5 Tg yr^{-1}, are distributed according to Price and Rind (1992). The model considers global NO emissions from fossil fuel burning on the order of 21 Tg N yr^{-1}, according to Benkovitz et al. (1996). CO emissions are distributed according to Lelieveld and van Dorland (1995), consisting of fossil fuel burning (450 Tg CO yr^{-1}), vegetation (100 Tg CO yr^{-1}), natural non-methane hydro-

Table 1. Location and dates of sonde launch during the 1995 INDOEX-cruise with the American R/V Malcolm Baldrige. Sondes were launched around noon local time

Sounding	Date	Latitude	Longitude
6	April 2, 1995	19.5 °S	55.0 °E
7	April 4, 1995	18.0 °S	55.0 °E
8	April 5, 1995	16.0 °S	55.0 °E
9	April 6, 1995	13.6 °S	55.0 °E
10	April 7, 1995	11.7 °S	54.1 °E
11	April 9, 1995	9.6 °S	51.9 °E
12	April 10, 1995	8.3 °S	52.3 °E
13	April 11, 1995	6.7 °S	52.9 °E
14	April 12, 1995	3.7 °S	55.0 °E
15	April 13, 1995	1.0 °S	55.0 °E
16	April 14, 1995	1.3 °N	56.7 °E
17	April 15, 1995	2.9 °N	58.2 °E
18	April 16, 1995	4.5 °N	59.7 °E
19	April 17, 1995	6.7 °N	61.7 °E
20	April 18, 1995	8.2 °N	63.0 °E
21	April 20, 1995	7.6 °N	73.1 °E

Table 2. Location and dates of sonde launch during the First Field Phase (FFP, 1998) INDOEX-cruise with the Indian R/V Sagar Kanya. Sondes were launched in the early afternoon or evening (local time)

Sounding	Date	Latitude	Longitude
1	Feb 23, 1998	8.0 °N	74.0 °E
2	March 2, 1998	0.2 °S	73.5 °E
3	March 4, 1998	4.3 °S	70.2 °E
4	March 6, 1998	8.1 °S	67.3 °E
5	March 8, 1998	11.1 °S	64.5 °E
6	March 10, 1998	16.1 °S	61.0 °E
7	March 13, 1998	20.1 °S	57.3 °E
8	March 18, 1998	12.4 °S	62.5 °E
9	March 19, 1998	11.0 °S	63.3 °E
10	March 20, 1998	7.1 °S	65.2 °E
11	March 22, 1998	3.0 °N	67.3 °E
12	March 24, 1998	2.4 °N	68.5 °E
13	March 27, 1998	11.4 °N	68.8 °E
14	March 28, 1998	14.1 °N	68.3 °E

carbon oxidation (280 Tg CO yr^{-1}), anthropogenic non-methane hydrocarbon oxidation (300 Tg CO yr^{-1}), oceanic emissions (40 Tg CO yr^{-1}), and wildfires (30 Tg CO yr^{-1}). The total NO and CO emissions considered in the model are 37.5 Tg NO yr^{-1} and 19 000 Tg CO yr^{-1}. Methane (CH$_4$) surface concentrations are prescribed, ranging from 1772 ppm in the northern hemisphere to 1680 ppm in the southern hemisphere.

The parameterization for dry deposition of O$_3$, NO$_X$ and HNO$_3$ is described in Ganzeveld and Lelieveld (1995) and Ganzeveld et al. (1998). The wet scavenging of HNO$_3$ and H$_2$O$_2$, CH$_2$O, CH$_3$OOH and HNO$_4$ is calculated using the large-scale and convective cloud and precipitation fields calculated on-line by the climate model as described by Roelofs and Lelieveld (1995, 1997).

The neglect of non-methane hydrocarbons on O$_3$ reduces the net global tropospheric O$_3$ production by 8% (Roelofs and Lelieveld, 2000). The differences are largest at mid-latitudes ($> 10\%$), smaller in the Indian Ocean free troposphere (5%), while becoming negative over the tropical Atlantic ocean (upto -5%).

Stratospheric O$_3$ mixing ratios are prescribed between 1 and 2 model layers above the tropopause up to the 10 hPa top level of the GCM. Transport of O$_3$ across the tropopause depend directly on the air motions simulated by the GCM. The simulated tropopause is marked by a potential vorticity of 3.5 10^{-6} K m^2 kg^{-1} s^{-2} poleward of 20° latitude (Hoerling et al., 1993), and by a -2 K km^{-1} temperature lapse rate equatorward of 20° latitude. Apart from O$_3$, the model considers a tracer for O$_3$ that originates from the stratosphere, referred to as O$_3$s. The tracer is treated similar to O$_3$, with the exception that no tropospheric production occurs. Thus, in the troposphere O$_3$s is only destroyed (reactions with OH and HO$_2$, photodissociation and surface deposition).

The model realistically represents the seasonal variability of the O$_3$ photochemical production and of O$_3$ transport from the stratosphere (Roelofs and Lelieveld, 1995, 1997). Surface O$_3$ mixing ratios as measured in remote and relatively clean conditions are also simulated by the model, but the model appears to underestimate the O$_3$ mixing ratios in some polluted regions because of neglect of non-methane hydrocarbon chemistry (Roelofs et al., 1997a; Roelofs and Lelieveld, 2000). The global average cross-tropopause O$_3$ flux (CTF) estimates range from 459 Tg O$_3$ yr^{-1} (Roelofs et al., 1997b), 495 Tg O$_3$ yr^{-1} (Roelofs and Lelieveld, 2000), 575 Tg O$_3$ yr^{-1} (Roelofs and Lelieveld, 1995), 590 Tg O$_3$ yr^{-1} (Roelofs and Lelieveld 2000) to 607 Tg O$_3$ yr^{-1} (Roelofs and Lelieveld, 2000). The differences are related to different chemistry schemes (with/without non-methane hydrocarbon chemistry; updated photodissociation rates; changes in the description of stratosphere-troposphere exchange). In Roelofs and Lelieveld (2000) the estimated range from other GCM model calculations yield cross-tropopause O$_3$ fluxes between 475 and 650 Tg O$_3$ yr^{-1}. Estimates based on correlation between several species (O$_3$, N$_2$O , ^{90}Sr, Potential Vorticity) range from 200 to 870 Tg O$_3$ yr^{-1}. At mid-latitudes the model might underestimate the CTF by 10–15% at the T30 resolution (Siegmund et al., 1996; Kentarchos et al., 2001), however, according to Siegmund et al. (1996) the CTF along the subtropical jets is over-estimated (up to 50%) at the current model resolution.

In this study, the so-called "nudging" technique (for this study the assimilation of ECMWF analysis data) was used
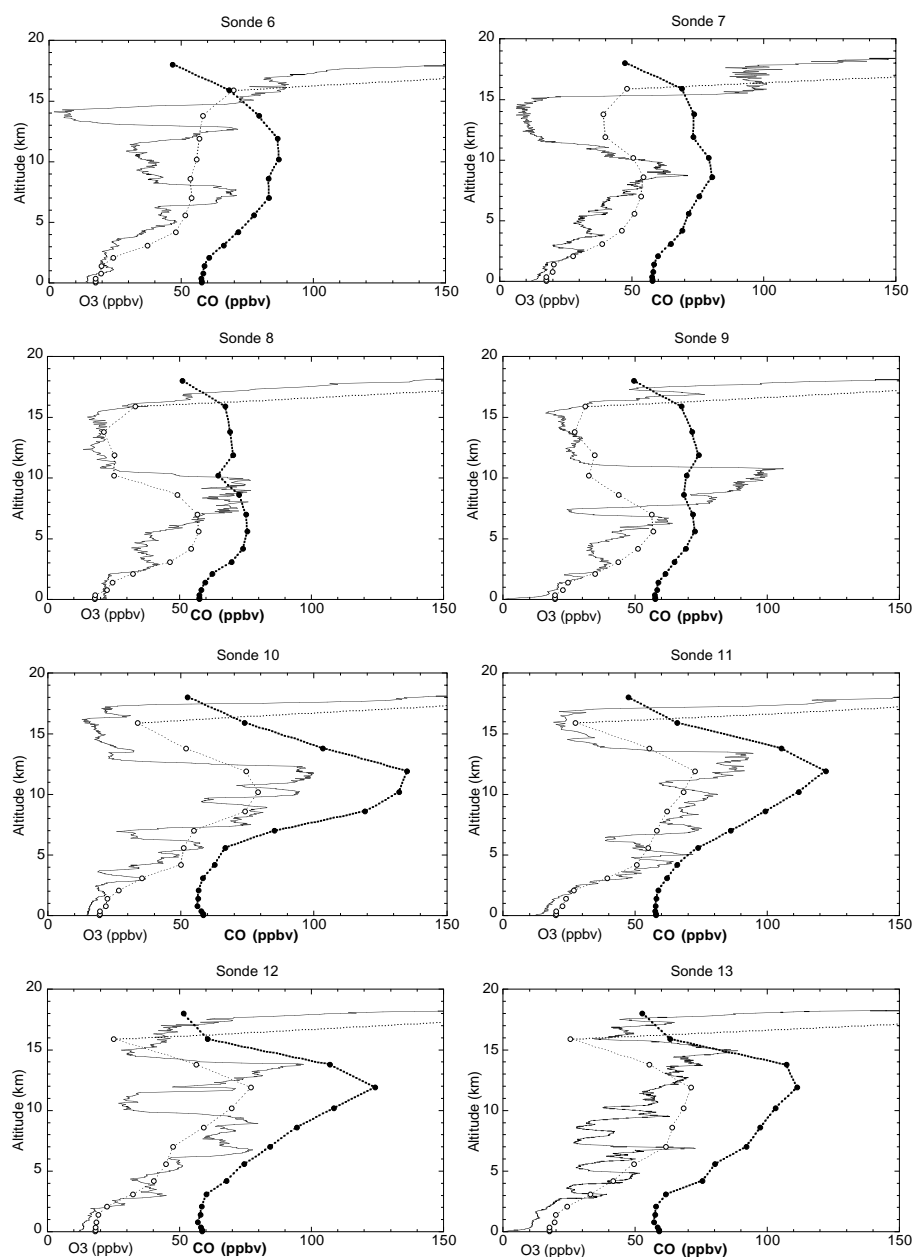
Fig. 2a. Vertical O$_3$ profiles from the 1995 INDOEX cruise profiles No 6 to 13 (solid thin lines), along with the corresponding O$_3$ (dashed thin line, open circles) and CO (dashed thick lines, filled circles) profiles from the ECHAM model. Mixing ratios are given in ppbv. For the location and launch time see Table 1.

to simulate specific periods. This method is described more extensively by Jeuken et al. (1996) and de Laat et al. (1999). The periods for which the ECHAM model was nudged in this study were 16 March – 30 April 1995, and 1 February – 1 April 1998. We note that the nudging method has been used for several other studies (Kentarchos et al., 1999, 2000, 2001; de Laat et al., 2001; de Laat and Lelieveld, 2000, 2002).

3   Observations

The O$_3$ profiles used in this study were obtained from two pre-INDOEX ship-campaigns. The first campaign took place

during March and April of 1995 with the R/V Malcolm Baldrige. From this campaign we used sixteen O$_3$ profiles that were measured along a track from Durban, South Africa to Colombo, Sri Lanka (Fig. 1). Surface measurements of several trace gases, aerosols and meteorological parameters were made along with the soundings. For a detailed description and results of this campaign see Rhoads et al. (1997) and de Laat et al. (1999).

The second campaign took place during February and March 1998 as part of the INDOEX First Field Phase (FFP), a larger preparatory campaign for the INDOEX Intensive Field Phase that would take place during the same months
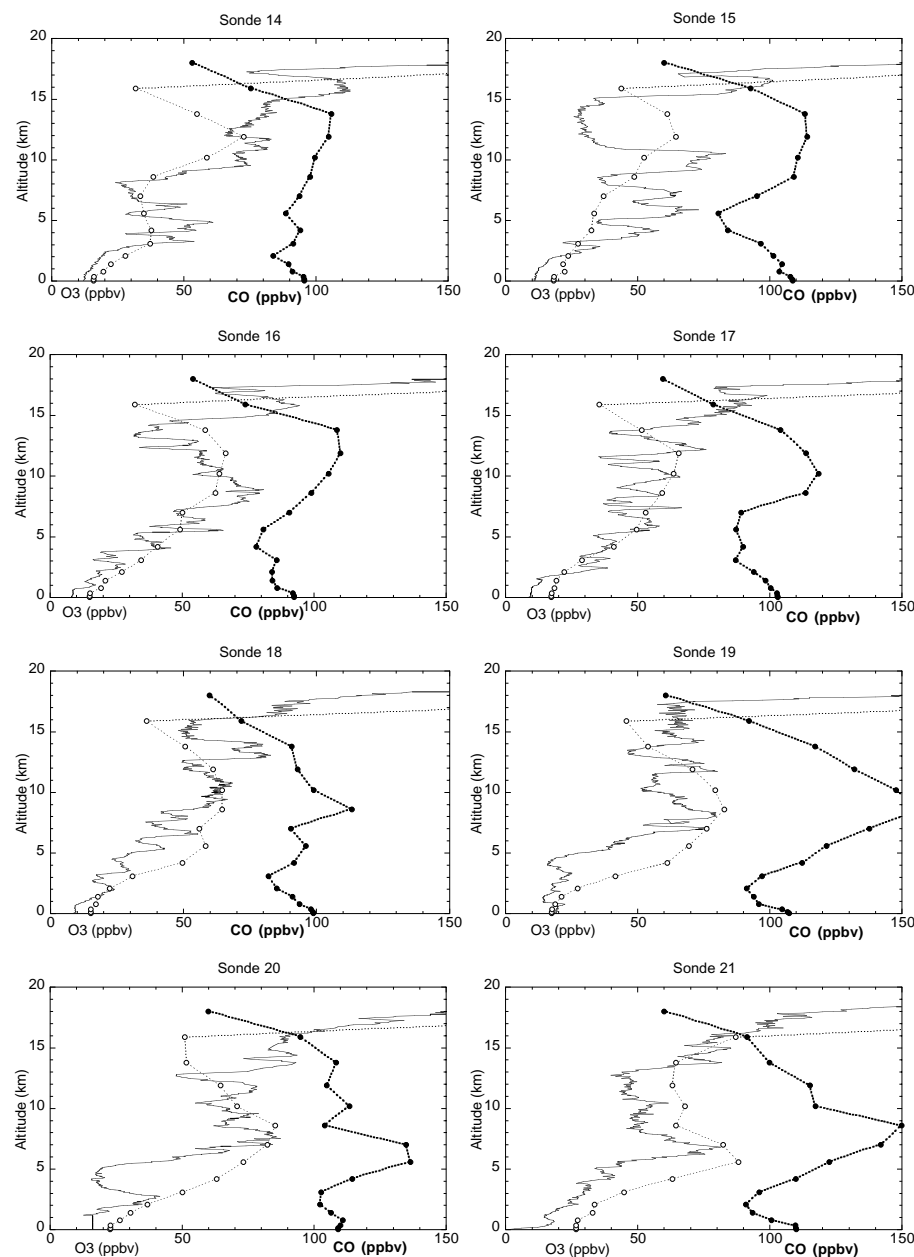
Fig. 2b. Similar to Fig. 2a but for profiles No 14 to 21.

one year later in 1999. The Indian R/V Sagar Kanya sailed from southern India to the Indian Ocean east of Madagascar (Fig. 2). As in the 1995 campaign, O$_3$ sondes were launched and surface measurements were made.

The O$_3$ sondes were balloon-borne Electrochemical Concentration Cell (ECC) O$_3$ sondes (model 1z, En-Sci Corp., Boulder, Colorado) coupled to Väisälä radiosondes (model RS80, Väisälä USA, Woburn, Massachusetts). The accuracy of the O$_3$ sensor varies from $\pm$ 1–2 ppbv below 5 km to $\pm$ 5 ppbv at 10 km and $\pm$ 20 ppbv at 20 km altitude (Smit et al., 1994, 1995). Tables 1 and 2 summarize the ship tracks and locations where the O$_3$ profiles were measured.

4   Measured and modeled O$_3$ profiles

4.1   1995 profiles

Figure 2a shows O$_3$ profiles measured from the ship cruise of R/V Malcolm Baldrige during March and April 1995. An analysis of profiles 6 to 13 can be found in de Laat et al. (1999). Profiles 9 and 10 are also discussed in de Laat and Lelieveld (2001). For the exact location of the O$_3$ profiles see Table 1. Profiles 6 to 13 were launched south of the ITCZ. The most striking features in profiles 6 to 13 are the low O$_3$ mixing ratios in the marine boundary layer (O$_3$ de-
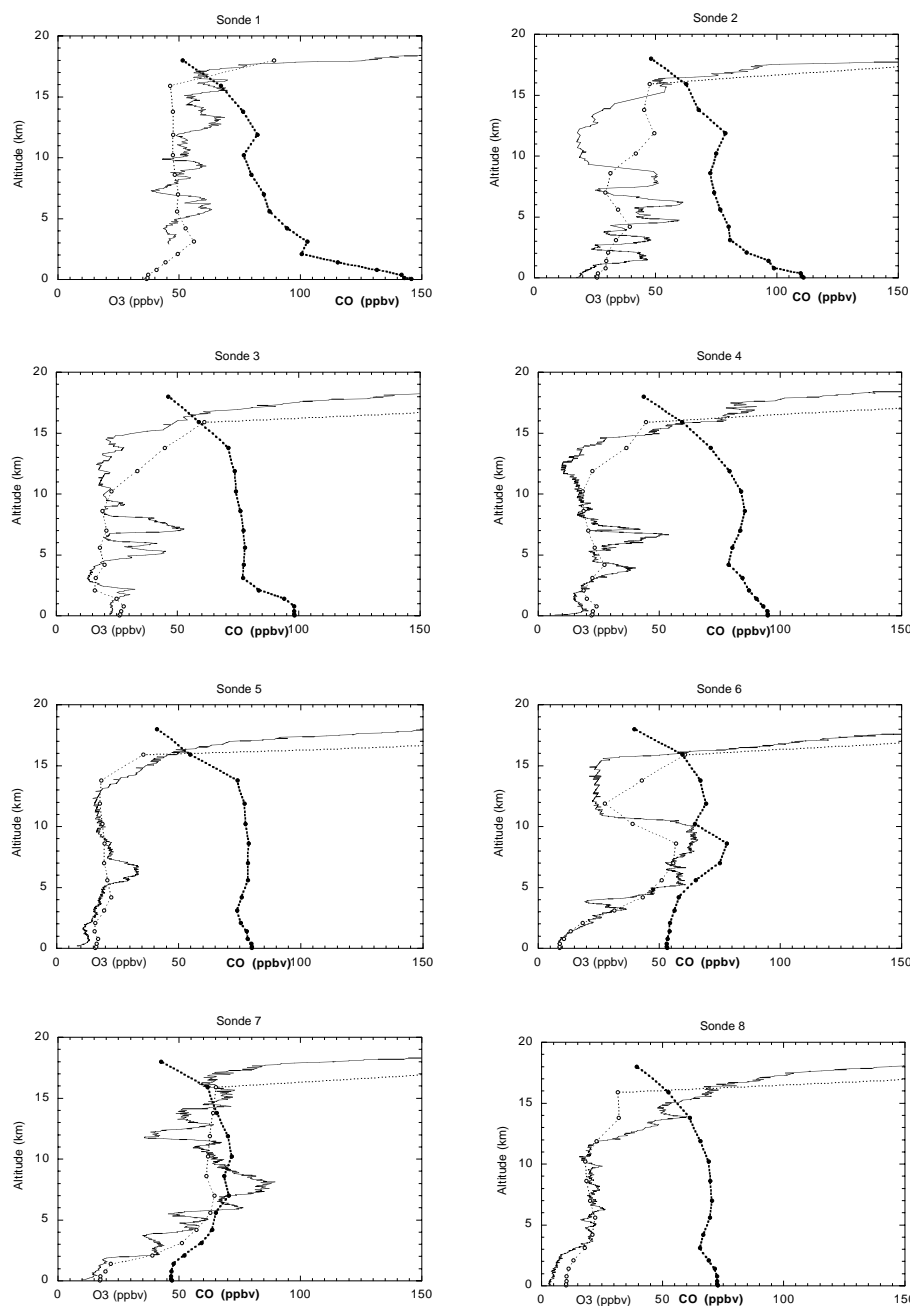
Fig. 3a. Similar to Fig. 2a but for the 1998 INDOEX profiles No 1 to 8.

structive environment), mid-tropospheric O_3 maxima, which can be attributed to biomass burning over Africa, and low upper-tropospheric O_3 mixing ratios, which are likely caused by vertical transport of marine boundary layer air due to convection. Furthermore O_3 laminae are present in most profiles between 14 and 17 km, most notably profiles 6 and 7. Figure 2a and b also show the modeled O_3 and CO profiles. The model simulates comparable absolute O_3 mixing ratios and the spatial and temporal variations as observed. The model cannot simulate smaller O_3 features in the profiles because of the low horizontal and vertical resolution. The low hori-

zontal resolution may cause some displacement of modeled gradient compared to actual location of the gradient because the observations were done in a region with sharp horizontal gradients. This may result in discrepancies between modeled and observed O_3 profiles (for example profile 9, see de Laat et al. (1999) for a detailed analysis). Modeled O_3 correlates well with modeled CO for mid-tropospheric O_3 maxima, indicating that the mid-tropospheric O_3 maxima have a tropospheric origin. Backtrajectory calculations showed that the air masses originated from biomass burning regions over central Africa (de Laat et al., 1999).
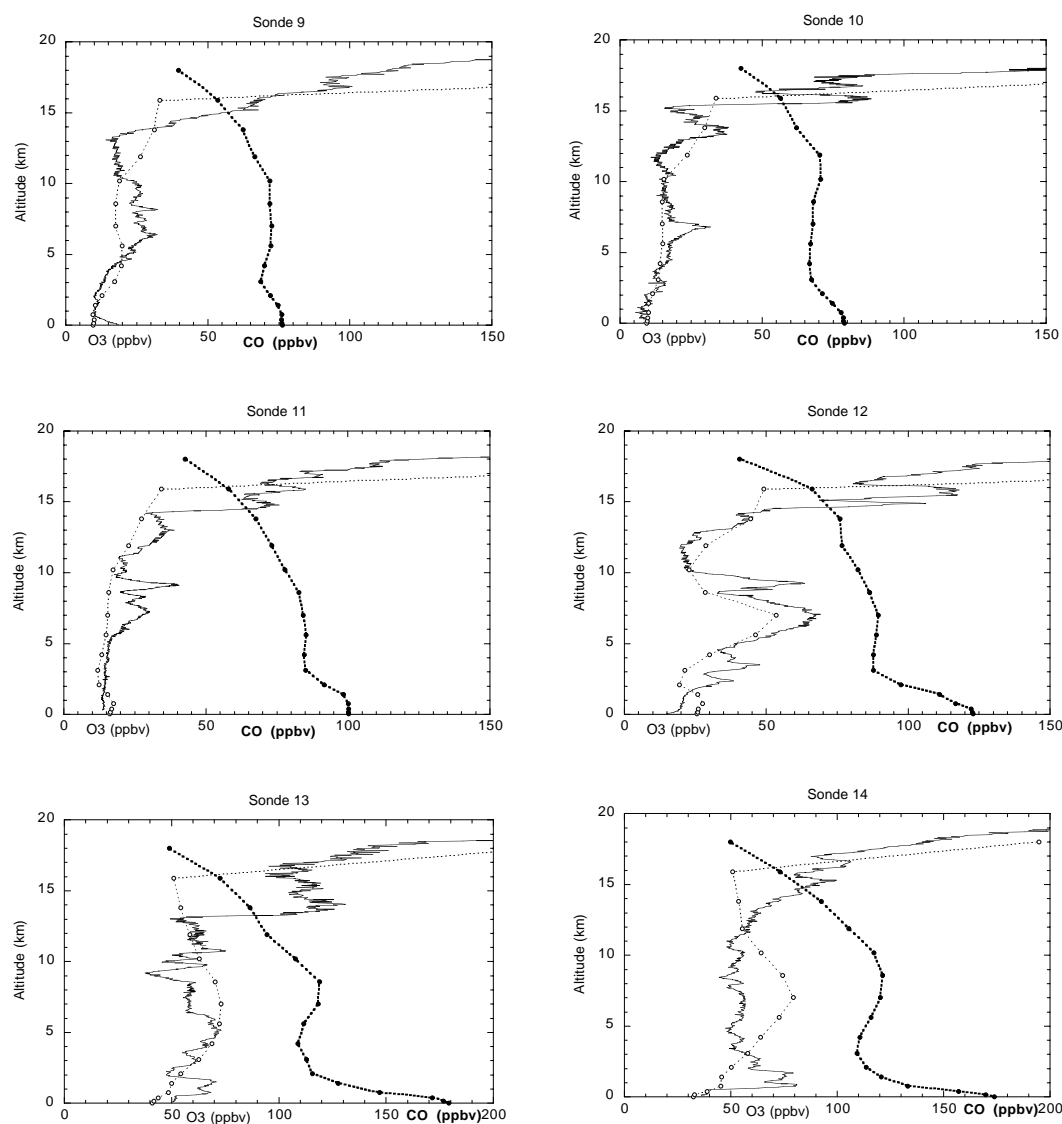
Fig. 3b. Similar to Fig. 2a but for 1998 INDOEX cruise profiles No 9 to 14.

Figure 2b also shows O_3 profiles from soundings launched during the 1995 cruise of the R/V Malcolm Baldrige, which have not been published before. The ITCZ was located close to profiles 14 and 15. Boundary layer O_3 is low, whereas free tropospheric O_3 is high. Upper-tropospheric O_3 minima are not as pronounced as in profiles 6 to 13, while they are clearly visible in the modeled profiles. Discrepancies between the measured and modeled profiles also occur close to the ITCZ (profiles 14 to 17). It can be expected that the model cannot simulate the exact location of the ITCZ at the current model resolution because generally the convective surface area (typically $10–1000$ km^2) is much smaller that the model gridsize (typically $100\,000$ km^2). Further away from the ITCZ (profiles 18 to 21) this is less of a problem.

Mid-tropospheric O_3 mixing ratios are generally high for all profiles, also north of the ITCZ, and are simulated by the model. As with profiles 6 to 13 in Fig. 2a, modeled mid-tropospheric O_3 peaks are associated with high model CO mixing ratios.

4.2 1998 (FFP) profiles

Figure 3a and b show vertical profiles from the 1998 IN-DOEX IFP O_3 soundings. An analysis of these profiles based on backtrajectory calculations and potential vorticity can be found in Zachariasse et al. (2000). For the details of the location and time of launch of these soundings see Table 2. The overall features of the 1998 profiles are similar to those measured in 1995: Low boundary layer O_3 mixing ratios, mid-tropospheric maxima and minima, and upper-tropospheric O_3 laminae between 14 and 17 km altitude. O_3 profiles mea-
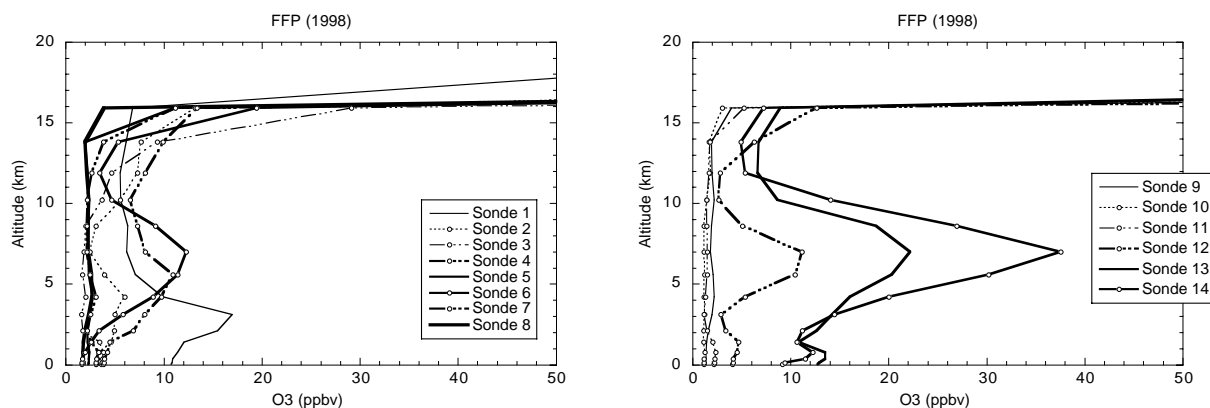
Fig. 4. Vertical profiles of O_3 of stratospheric origin (O_3s) from the ECHAM model, for the 1998 profiles. The left panel shows 1998 profiles 1–8, the right panel shows profiles 9–14. Mixing ratios in ppbv.

sured at close locations during both years are very similar (1995 profiles 7 to 9 and 1998 profiles 6 and 7). However, mid-tropospheric O_3 mixing ratios are generally lower for the FFP-profiles than for the 1995 profiles. Modeled O_3 profiles are similar to measured O_3 profiles. Large discrepancies only exist for profile 14, with an observed mid-tropospheric minimum and a modeled mid-tropospheric maximum, and profile 2, for which the model does not simulate the observed upper-tropospheric minimum. Similar to the 1995 profiles, the model does not capture the upper-tropospheric O_3 laminae very well, but no upper tropospheric O_3 minima are present in the modeled profiles, with the exception of profiles 13 and 14. Furthermore, O_3 mixing ratios increase from an altitude of 12 km and higher for most modeled profiles.

Modeled CO profiles corresponding to the measured O_3 profiles are somewhat different to the modeled 1995 CO profiles. Generally, modeled mid-tropospheric CO mixing ratios are lower during 1998 than during 1995. This corresponds with lower mid-tropospheric O_3 mixing ratios for the 1998 profiles, which one would expect if O_3 and CO have the same source. Boundary layer CO mixing ratios north of the ITCZ are higher compared to 1995. Considering that the FFP profiles were measured earlier in the year (March) compared to 1995 (April), the discrepancies can be explained as follows. According to de Laat and Lelieveld (2002) the strength of the boundary layer continental outflow from India to the Indian Ocean weakens considerably during March and April, lowering the boundary layer levels of pollution. Furthermore, the convective outflow in the free troposphere (divergent flow away from the convection) at the ITCZ will be balanced by the mid-tropospheric inflow of polluted air masses from the subtropics. A weak ITCZ allows the polluted free tropospheric subtropical air masses north and south of the equator to be advected further equatorward than in case of a strong ITCZ. The ITCZ is generally stronger during March than during April over the Indian Ocean. Therefore, more boundary layer air is vertically mixed at the ITCZ during March

than during April. Furthermore, a stronger ITCZ causes a stronger divergent upper-tropospheric flow that can transport the "clean" air masses further away from the ITCZ. Thus, free tropospheric O_3 and CO mixing ratios will be lower and cover a larger area during March compared to April. The result is that free tropospheric O_3 and CO mixing ratios are lower for the 1998 profiles compared to the 1995 profiles.

The ECHAM model also provides a separate tracer for O_3 that originates from the stratosphere (hereafter O_3s). The influence of STE along the subtropical jets on tropospheric O_3 can be derived for the modeled profiles using this tracer. Figure 4 shows modeled O_3s profiles for the 1998 soundings. With the exception of profiles 13 and 14, the contribution of O_3s to total tropospheric O_3 is relatively small (less than 20%, cf. Roelofs and Lelieveld, 1997). On the other hand, the mid-tropospheric O_3 features in profiles 6, 7, 12, 13 and 14 are at least partly of stratospheric origin. The contribution of O_3s can be as high as 50% for profiles 13 and 14.

Modeled CO mixing ratios above 12 km altitude decrease to approximately 50 to 60 ppbv around 18 km altitude (see Figs. 2 and 3). Modeled free tropospheric CO mixing ratios higher than 50 to 60 ppbv indicates a tropospheric origin, while lower mixing ratios indicate a stratospheric origin (unless O_3 mixing ratios are low, which indicates vertical mixing of very clean marine boundary layer air masses). Such low CO mixing ratios are not modeled for any of the 1998 (or 1995) profiles. Interestingly, the highest O_3s contribution is modeled for profiles 13 and 14, which also showed the highest mid-tropospheric CO mixing ratios modeled for 1998. Based on the modeled profiles and the correlation between O_3 and CO peaks for both 1995 and 1998 we can conclude that the major sources of mid-tropospheric O_3 maxima are of tropospheric origin. According to 1998 profiles 13 and 14, there also may be a relation between STE and the advection of O_3 and CO rich tropospheric air.

5 Mid-tropospheric O$_3$ and CO maxima: source region and advection mechanism

The model-observation comparison yields that the source of the mid-tropospheric O$_3$ and CO maxima could very well be tropospheric. Using the model we can try to determine what the source regions are and how the pollution is advected to the Indian Ocean. For that, we first need to understand the dynamical processes in this region. Africa is an important source region of pollutant emission of NO$_X$ and CO (Crutzen and Carmichael, 1993; Roelofs et al., 1997a). In particular, biomass burning is the major source of these pollutants (Crutzen and Andrae, 1990; Crutzen and Carmichael, 1993; Hao and Liu, 1994; Galanter et al., 2000; de Laat et al., 2001). CO production will also occur indirectly by way of oxidation of higher hydrocarbons, which are additionally emitted by biomass burning. The biomass-burning season in Africa is very much dependent on the time of year (Hao and Liu, 1994). Generally, biomass burning occurs during the local dry season, causing a maximum in pollution levels. CO mixing ratios are highest near the surface, and lower in the free troposphere aloft. On the other hand, tropospheric O$_3$ is mostly produced by a catalytic reaction chain involving NO$_X$ (e.g. Graedel and Crutzen, 1993). Not only will O$_3$ be produced close to the source regions of its precursors, but as the precursors are transported, it will also be produced during advection (Chatfield and Delaney, 1990; Pickering et al., 1992). This so-called "mix-then-cook" mechanism, in combination with O$_3$ removal that occurs at the surface, causes O$_3$ mixing ratios to be generally higher in the free troposphere than at the surface. Furthermore, free tropospheric pollution is mostly removed by reaction with OH. In turn, OH depends largely on the presence of moisture (H$_2$O). Because moisture decreases with altitude, the lifetime of O$_3$ and its precursors CO and NO$_X$ can become quite long, enabling plumes of pollution to travel long distances, especially under dry conditions as they occur in the descending branches of the Hadley circulation.

There exists a distinct difference in the tropospheric chemical composition over Africa between regions north and south of the equator due to differences in meteorology, emissions and photochemistry. Major convection occurs south of the equator during the winter monsoon period (Hastenrath, 1988), following the maximum in solar insolation, while biomass burning mainly occurs north of the equator (Hao and Liu, 1994). The maxima in average modeled surface O$_3$ and CO mixing ratios for February and March 1998 occur north of the ITCZ, caused by high pollutant emissions (dry season) and active photochemistry (less clouds). At 10 km altitude only a maximum in CO is simulated, and it is located further south. Ostensibly the maximum mixing ratios at the surface and in the free troposphere should occur at the same (geographical) location. However, although maximum surface pollution occurs north of the ITCZ, surface pollution levels over Austral Africa are still high (> 200 ppbv). Hence the upper-tropospheric CO maximum simply reflect the convective areas. Actually, because there is a latitudinal pollution gradient at the surface over Austral African, the maximum free tropospheric CO mixing ratios are found over the area where both convection and the highest surface pollution levels occur (Fig. 5). For O$_3$ it is more difficult to distinguish a free tropospheric maximum, due to the influence of stratospheric O$_3$ and the ongoing O$_3$ formation, that can occur after air masses are advected away from the convection. However, subtracting the modeled stratospheric O$_3$ tracer from total O$_3$ yields the amount of O$_3$ that is produced in the troposphere. Figure 6 shows the average residual O$_3$ mixing ratios at 10 km altitude for February and March 1998. Maximum mixing ratios occur over Africa and the tropical Atlantic, although the region with high mixing ratios is more widespread for residual O$_3$ than for CO, reflecting the different source mechanisms for both species.

Figure 5 also shows that at the 10 km altitude level CO is advected (on average) from central Africa along the northern and southern hemispheric subtropical jets (NH-STJ and SH-STJ) at 20°–30° towards the Indian Ocean. A similar pattern exists for residual O$_3$ along NH-STJ (Fig. 6). Advection of O$_3$ from central Africa also occurs along the SH-STJ during February 1998, while it appears to be absent in CO during the same month. However, this probably is a spurious observation reflecting the very nature of upper-tropospheric CO. Free tropospheric CO mixing ratios (as well as residual O$_3$, see Fig. 6) are lower during February compared to March 1998 due to lower convective activity. Hence less pollutants are transported from the boundary layer to the troposphere. At the same time STE will transport CO depleted air to the troposphere along the SH-STJ. Consecutive mixing between stratospheric and tropospheric air lowers CO mixing ratios, masking the "CO-pollution" plume which is visible in the residual O$_3$ field along the SH_STJ.

The mechanism responsible for the advection along the subtropical jets can be determined from Figs. 7a and b, showing modeled O$_3$, CO, O$_3$s and O$_3$t and the wind fields for two days during March 1998 at 10 km altitude (10 and 13 March, Day of Year (DOY) 69 to 72). For clarity, only CO mixing ratios above 100 ppbv, O$_3$ mixing ratios above 70 ppbv, O$_3$s mixing ratios above 50 ppbv and O$_3$t mixing ratios above 40 ppbv are shown.

On DOY 69, high CO mixing ratios are located over central Africa with corresponding O$_3$ mixing ratios reaching 70 ppbv. A wave in the NH-STJ is approaching from the west (at 0° E), causing winds in front of the wave to change from westerly to southwesterly. The divergent flow (convective outflow) at 10 km altitude over central Africa is relatively constant. Therefore, the wave at the STJ causes an acceleration of the flow just south of the wave. This initiates advection of polluted African air masses. North and south of the NH-STJ O$_3$ mixing ratios are high, reflecting the change in the height of the tropopause north and south of the STJ. Moreover, at the latitude with the highest wind speeds the
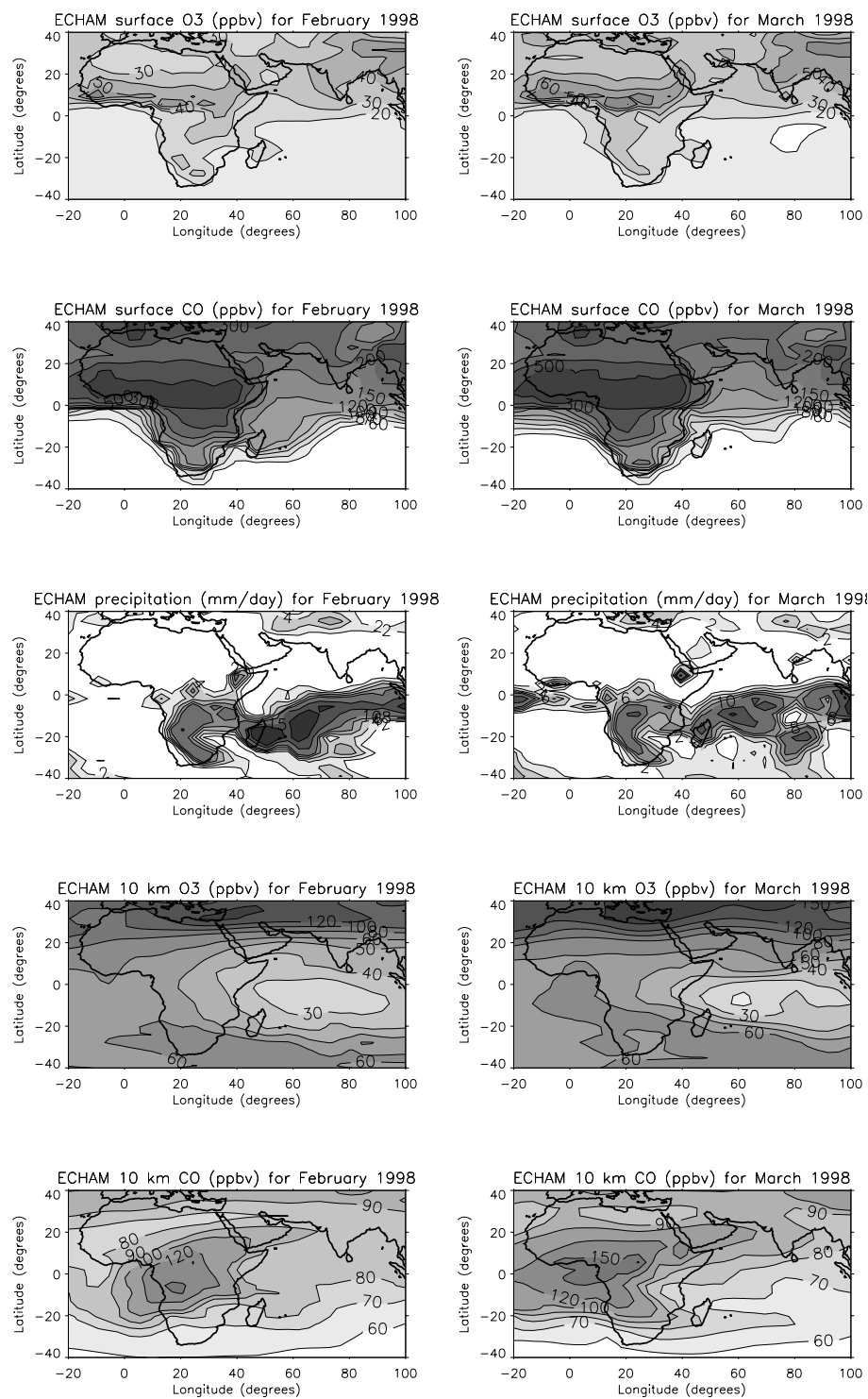
Fig. 5. Monthly averaged ECHAM results for the INDOEX region, February and March 1998: surface O_3 and CO, precipitation and 10 km altitude O_3 and CO. Mixing ratios in ppbv, precipitation in mm day^{-1}.

largest gradients in O_3 occur. At the SH-STJ the increase in O_3 mixing ratios is not as distinct as along the NH-STJ. No east-west oriented latitudinal O_3 gradient exists along the SH-STJ, opposite to the NH-STJ. High O_3 mixing ratios occur in bands that are associated with the frontal zones of low

mid-latitude low-pressure areas. The cross-frontal circulation causes strong downward motions just behind the front, transporting O_3 from the stratosphere to the troposphere. The differences in O_3 mixing ratios along the NH-STJ and SH-STJ reflect the differences in the dynamical structure of the
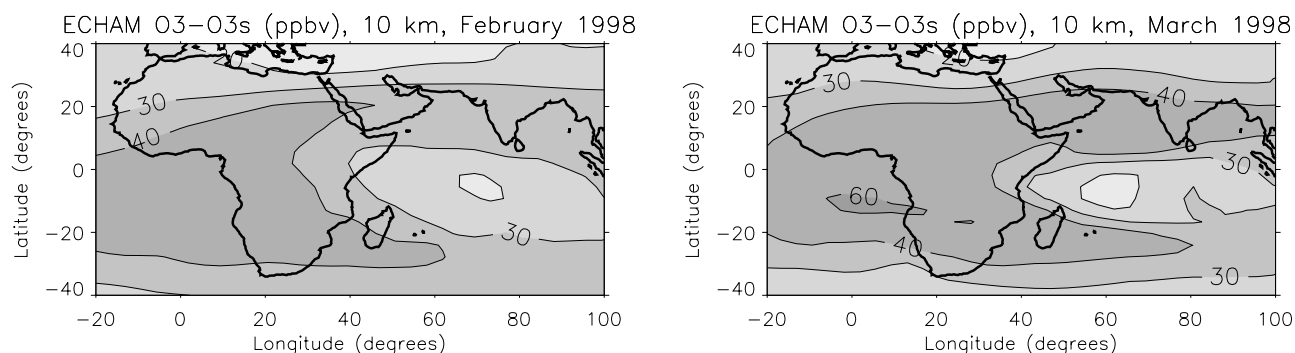
Fig. 6. Monthly averaged ECHAM residual O$_3$ (O$_3$ minus O$_3$s) for February and March 1998 at 10 km altitude in ppbv.

STJ. The NH-STJ is generally stronger and more persistent than the SH-STJ (Hastenrath, 1998), which results in an east–west oriented NH-STJ and a more meandering SH-STJ. At the same time, a band with high O$_3$ is located along the SH-STJ over the southern tip of Africa (30° S, 25° E). Winds change from southwest to west at this band, indicative of a frontal zone.

On DOY 72 the wave along the NH-STJ has advanced to the Arabian Sea, with advection of CO-rich air masses in the wake of the wave. The polluted air masses have advanced to over India. In the wake of the wave the circulation changes from westerly to northwesterly, thereby injecting the polluted air masses into the tropics. At the same time O$_3$s descends into the tropical troposphere at the wave, but remains north of the African pollution. This STE over India may be enhanced by the interaction of the wave with the Himalayas and/or the Tibetan plateau. The frontal zone along the SH-STJ has advanced to 70° E. Polluted African air masses are advected eastward north of the frontal zone. O$_3$s is transported downwards south of the frontal zone. The high O$_3$t mixing ratios are clearly associated with high CO mixing ratios. Furthermore, high O$_3$s and O$_3$t mixing ratios do not occur simultaneously, but are somewhat separated.

As both the "northern wave" and the "southern front" continue to advance further east, the flow along the subtropical jets becomes westerly again, which will shut down the advection of polluted air masses from central Africa, while at the same time STE vanishes. Polluted air masses (CO and O$_3$, the latter both from tropospheric and stratospheric origin) have entered the descending branches of the Hadley circulation, and will be slowly advected towards the ITCZ. The pollution is gradually removed during this advection.

This sequence occurs every time waves or fronts travel along the subtropical jets. It is important to note that, as these fronts have passed the African continent, they will be rich in O$_3$ both poleward (stratospheric O$_3$) and equatorward (tropospheric pollution) of the subtropical jets. Therefore, high free tropospheric O$_3$ mixing ratios over the Indian Ocean are not an indication of a stratospheric origin, even though trajectories indicate advection along the subtropical jets. Low humidity is also not an indicator for a stratospheric origin because air masses dry out very rapidly in the downward branch of the Hadley circulation. Frontal mixing of air masses may complicate the situation even more.

6 Summary and discussion

The analysis of model simulations reveals the mechanism behind the mid-tropospheric O$_3$ peaks in the downward branches of the Hadley circulation. During the winter monsoon period a mid and upper-tropospheric "reservoir" of polluted air masses with high O$_3$ and CO mixing ratios is present over central Africa. This "reservoir" is fueled by surface emissions in equatorial Africa. Upper-tropospheric divergence due to convective outflow causes the pollution to slowly propagate north and south over Africa. Waves or frontal zones propagate along the subtropical jets and cause winds along the equatorward edges of the STJ to change from an east–west direction to south-west (NH) or north–west (SH). This causes advection of polluted air masses from the African reservoir to the edge of the subtropical jets. At the STJ the polluted air masses are advected eastward in front of the frontal zone. The polluted air masses enter the downward branches of the Hadley circulation over the Indian Ocean, causing an increase in O$_3$ and CO mixing ratios. In addition to this mechanism air masses of stratospheric origin may enter the troposphere at the back of the frontal zones that propagate along the STJ. However, the model simulations also indicate that O$_3$s is not advected that deep into the tropics. Furthermore, due to their slow downward motion over the subtropical Indian Ocean the polluted tropospheric air masses dry out. This results in very low humidity, which could easily be misinterpreted as a stratospheric signature, while it is simply a result of local dynamics. Figures 8 and 9 further illustrate the relationship between O$_3$ and CO by showing the correlations between modeled CO, O$_3$, O$_3$s and residual O$_3$. Figure 8 shows a latitudinal cross-section between 45° S and 35° N along 69° E for February and March 1998. Several different regimes can be distinguished.
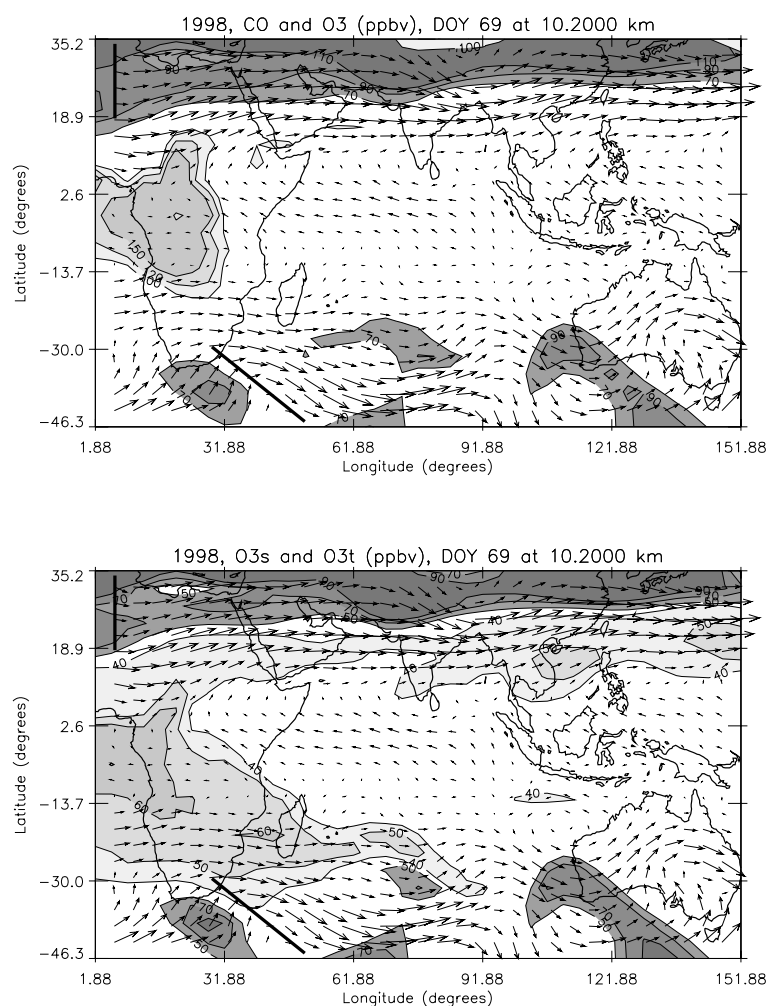
Fig. 7a. ECHAM model results at 10 km altitude over the INDOEX region for 10 March (DOY 69, 00:00 GMT): wind field in arbitrary units. Upper panel: CO (contour intervals: 100, 120 and 150 ppbv) in lighter colors, O_3 (contour intervals: 70, 90 and 110 ppbv) in darker colors. Lower panel: O_3t (contour intervals: 40, 50, and 60 ppbv) in lighter colors, O_3s (contour intervals: 50, 70 and 90 ppbv) in darker colors. The location of the two waves/frontal zones that are described in the text are indicated by the thick black lines.

In the tropopause region there is a negative correlation between CO and O_3/O_3s. Tropospheric O_3 mixing ratios are relatively low compared to stratospheric O_3 mixing ratios, while tropospheric CO mixing ratios are high compared to stratospheric CO mixing ratios (CO is photodissociated in the stratosphere). This causes a negative correlation between CO and O_3. This is also reflected in the positive correlation between CO and residual O_3 (O_3t).

In the southern hemispheric MBL the correlation between CO and O_3 is negative, also for residual O_3. These air masses can be considered "clean". O_3 and CO mixing ratios are low. CO mixing ratios are mainly determined by OH breakdown because sources are small. The OH concentration is strongly dependent on O_3 mixing ratios. Thus, if O_3 is low, OH concentrations will be low hence CO removal will be low and CO mixing ratios remain higher. Vice versa, if O_3 is higher, OH will be higher and CO mixing ratios will be lower.

At the ITCZ there is a positive correlation between CO and O_3. North of the ITCZ air masses are polluted with high CO and O_3 yields. In polluted air masses CO and O_3 have a posi-

tive correlation: more pollution (more CO) leads to more O_3. At the same time, southern hemispheric air masses are clean, and compared to northern hemispheric air masses, relatively low in O_3 and CO. Thus, changes from SH to NH air masses cause a similar change in both CO and O_3. Since this positive correlation also exists for CO and O_3s, the Indian subcontinent apparently is also a "source" of stratospheric O_3. Note however that the high correlation does not mean that O_3s is abundant.

Higher up (in altitude) at the ITCZ the CO-O_3 correlation becomes negative. Compared to the MBL the free troposphere is high in O_3, but low in CO. Thus, if MBL air masses are mixed vertically, O_3 mixing ratios will decrease whereas CO mixing ratios will increase.

In the free troposphere north of the equator two regimes can be identified. At 20° N a "tongue" of negatively correlated CO and O_3s descends into the troposphere .This is stratospheric air entering the troposphere (hence the negative correlation). At the same time, there is a positive correlation between CO and residual O_3, caused by the advec-
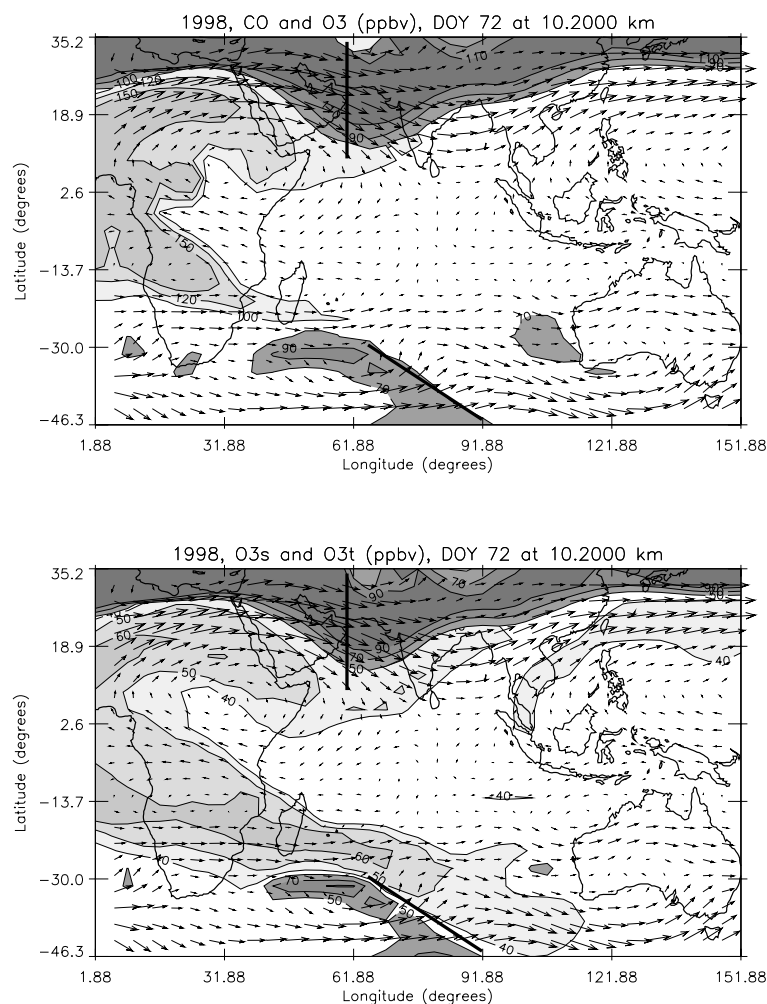
Fig. 7b. Similar to Fig. 8a, but for 13 March (DOY 72 00:00 GMT).

tion of polluted African air masses. Close to the equator the CO-O$_3$s correlation becomes positive, indicating some mixing between stratospheric air masses and polluted African air masses.

The tropospheric origin of free tropospheric air masses over India is also reflected in Fig. 9, showing the correlations at 8.6 km altitude for the INDOEX region. For CO and O$_3$ the regions with high correlations are small, but they reflect the ambiguous nature of the air masses of free tropospheric air masses. A positive correlation (tropospheric) exists over eastern Africa towards southern India, while over northern India the correlation is negative (stratospheric). This pattern is more pronounced in the CO-O$_3$s and CO-residual O$_3$ correlation. CO is strongly correlated with residual O$_3$ and strongly anti-correlated with stratospheric O$_3$. Only close to the CO-source region (convection over Austral Africa) these correlations become small, due to the different chemical nature of CO and O$_3$ close to pollution sources. The positive correlation between CO and O$_3$s just east of equatorial Africa could be caused by the mixing that of African pollution and

stratospheric air in the free troposphere over India. The general flow at the equator is westward, transporting the free tropospheric Indian air masses towards Africa. However, note that in tropical equatorial regions the contribution of O$_3$s to total O$_3$ is small ($< 10\%$, Roelofs and Lelieveld, 1997).

There exist other studies that yield additional clues to African pollution as source of free tropospheric O$_3$ over the Indian Ocean. The analysis of Thompson et al. (1996) and Chatfield et al. (1996) for the SAFARI (Southern Africa Fire Atmospheric Research Initiative) and TRACE A (Transport and Atmospheric Chemistry Near the Equator-Atlantic) campaigns show a remarkable resemblance with the analysis presented in this study, even though the above mentioned studies were carried out for October 1992. Part of the mid-tropospheric air masses over central and southern Africa are advected southeast and subsequently along the SH-STJ eastward over the southern Indian Ocean (plate 3 and 4 of Thompson et al., 1996; Fig. 1 of Chatfield et al., 1996). Furthermore, part of the air masses are also advected to northern Africa and then along the NH-STJ eastward over southern
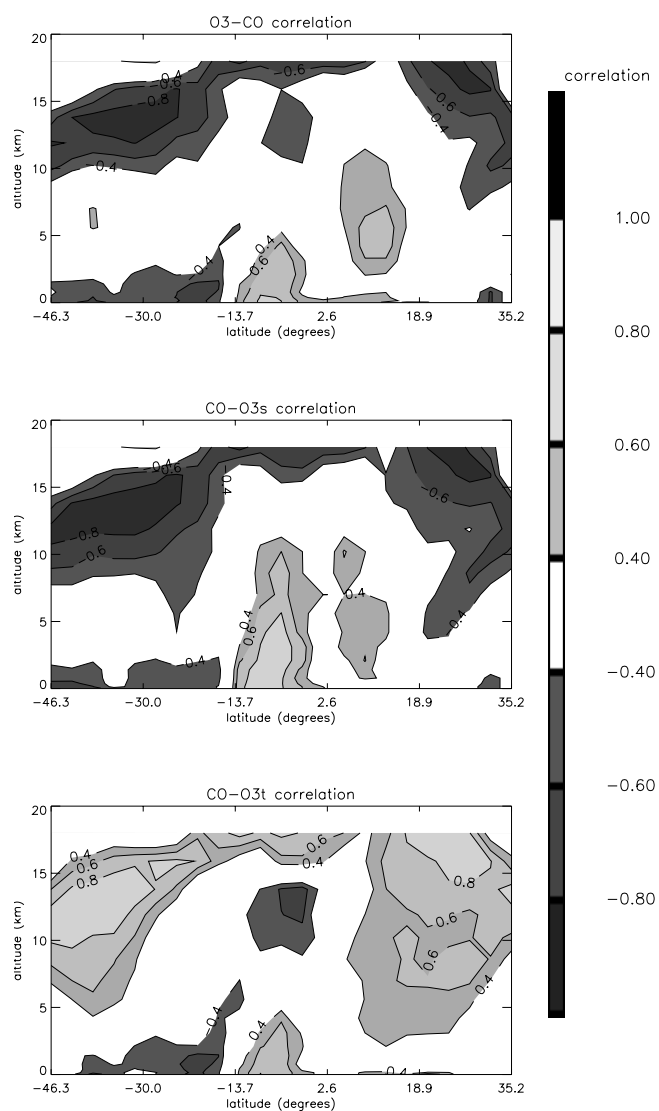
Fig. 8. Correlation coefficients between modeled **(a)** CO and O_3, **(b)** CO and O_3s and **(c)** CO and residual O_3 (O_3–O_3s) for a latitudinal cross-section along 69° E, between 45° S and 35° N, 0 and 20 km altitude, February and March 1998.

Fig. 9. Correlation coefficients between modeled **(a)** CO and O_3, **(b)** CO and O_3s and **(c)** CO and residual O_3 (O_3–O_3s) for the IN-DOEX region at 8.6 km altitude, February and March 1998.

Asia (plate 4 of Thompson et al., 1996).

The model simulates the average profile structure as measured, although discrepancies exist. There may be several different reasons for the existence of the discrepancies: missing or wrong chemistry, missing or wrong advection processes, errors in the ECMWF analyses, etc. However, the existence of discrepancies does not necessarily mean that the model results are "wrong". In order to "believe" the model result they must meet two criteria: the model should be able to simulate the average measured mixing ratios, and the model should be able to simulate the spatial and temporal
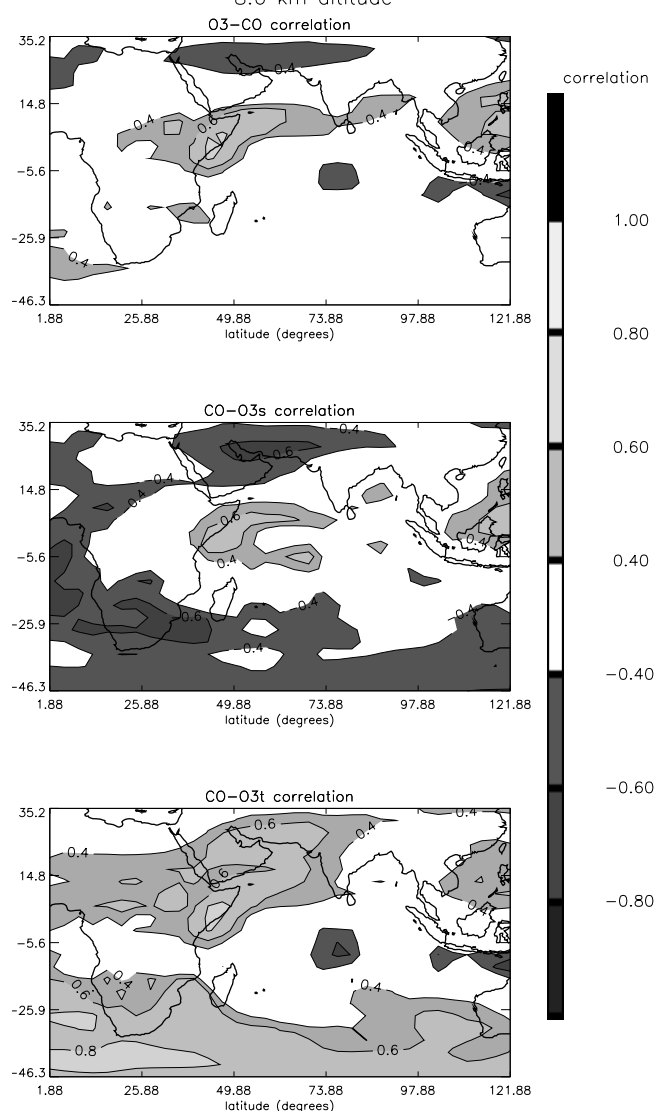
variability as observed. The model does simulate the average O_3 mixing ratios for most profiles. More importantly, it also simulates the spatial variability. Note for example that 1998 profiles 5 and 6 are taken at a distance of approximately 6° degrees. At T30 resolution that is less than two gridpoints. Mid-tropospheric O_3 mixing ratios increase from 20 ppbv in profile 5 to 6 ppbv in profiles 6. The model simulates both profiles, showing that it is capable of capturing the observed variability.

There is a striking discrepancy between measured and modeled O_3 in 1998 profile 14 (and to a lesser extent in profile 13): in the measured profile there is a mid-tropospheric

O$_3$ minimum, whereas in the modeled profile there is maximum. This hints at a mis-representation of one or more processes in the model. The (measured) maximum just above the boundary layer is though to be related to the local sea breeze circulation at the Indian Coasts (de Laat et al., 2001; Leon et al., 2001). Similar layers have also been reported for aerosol measurements (Leon et al., 2001; Müller et al., 2001; Reiner et al., 2001), CO (de Laat et al., 2001; Reiner et al., 2001), acetone, acetonitrile and SO$_2$ (Reiner et al., 2001). The sea breeze circulation causes polluted continental air masses to be lifted above the (marine) boundary layer after which they are advected from the continent to the ocean. The pollution will be restricted to a shallow layer above the (marine) boundary layer because of the large-scale subsidence over the northern Indian Ocean (the downward branch of the Hadley circulation). The ECHAM model resolution is too coarse to simulate the sea-breeze circulation. Disregarding this maximum (which is smaller in profile 13: further away from the continent), the tropospheric O$_3$ profile is more or less constant up to 12 km altitude. Figure 4 showed that for modeled 1998 profiles 13 and 14 there was large contribution of O$_3$s, caused by the passage of a wave in NH-STJ over northern India. Apparently the contribution of O$_3$s is too large in the model, which fits in nicely with a study by Siegmund et al. (1996), who showed that at the current model resolution (T30) the cross-tropopause flux (CTF) along 30° N is larger compared to simulations at higher resolutions. It is believed that the models more realistically simulate the CTF at higher horizontal resolution. In addition, the model may have problems simulating the exact location of the event. A displacement could cause spurious advection of O$_3$s.

7 Conclusions

In this study I have shown that the nudged ECHAM model realistically simulates O$_3$ profiles from two pre-INDOEX campaigns, both their spatial and temporal variability. The subtropical Indian Ocean atmosphere outside the ITCZ consists of low boundary layer O$_3$, mid-tropospheric O$_3$ maxima, either O$_3$ minima or maxima at the convective outflow region (8–12 km), and O$_3$ laminae between the convective outflow region and the tropopause. At the ITCZ O$_3$ mixing ratios are generally low throughout the troposphere due to extensive vertical mixing of MBL air masses by convection. The model simulations show that for the mid-tropospheric O$_3$ maxima CO mixing ratios are high as well. The major source region of the enhanced CO mixing ratios is free tropospheric African pollution. The pollution is advected from the source regions over equatorial Africa towards the subtropical jets, then along the subtropical jets towards the Indian Ocean, where part of the pollution enters the descending branches of the Hadley circulation at subtropical latitudes. The advection along the subtropical jets is closely related to the passage of waves and frontal zones along the subtropical

jets. Such waves or fronts cause an acceleration of the flow and advection of polluted tropical air masses, while at the same time also cause transport of stratospheric air masses to the troposphere. However, the mode simulations show that stratospheric air masses remain at higher latitudes; generally they do not advance deep into the tropics. The discrepancy between measured and modeled O$_3$ profiles close to India in 1998 is most likely related to the too high CTF along the subtropical jet. Other discrepancies in O$_3$ profile shape between observations and model simulations are attributed to the model resolution.

References

Baray, J. L., Ancellet, G., Randriambelo, T., and Baldy, S.: Tropical cyclone Marlene and stratosphere-troposphere exchange, J. Geophys. Res., 104, 13 953–13 970, 1999.

Baray, J. L., Randriambelo, T., Baldy, S., and Ancellet, G.: Comment on "Tropospheric O$_3$ distribution over the Indian Ocean during spring 1995 evaluated with a chemistry-climate model" by de Laat, A. T. J., et al., J. Geophys. Res., 106, 1365–1368, 2001.

Benkovitz, C. M., Scholtz, M. T., Pacyna, J., Tarrason, L., Dignon, J., Voldner, E. C., Spiro, P. A., Logan, J. A., and Graedel, T. E.: Global gridded inventories of anthropogenic emissions of sulfur and nitrogen, J. Geophys. Res., 101, 29 239–29 254, 1996.

Chatfield, R. B. and Delaney, A. C.: Convection links biomass burning to increased tropical ozone: However, models will tend to overpredict O$_3$, J. Geophys. Res., 95, 18 473–18 488, 1990.

Chatfield, R. B., Vastano, J. A., Singh, H. B., and Sachse, G.: A general model on how fire emissions and chemistry produce African/oceanic plumes (O$_3$, CO, PAN, and smoke) in TRACE A, J. Geophys. Res., 101, 24 791–24 306, 1996.

Chen, C. T. and Roeckner, E.: Validation of the earth radiation budget as simulated by the Max Planck Institute for Meteorology general circulation model ECHAM4 using satellite observations of the Earth Radiation Budget Experiment, J. Geophys. Res., 101, 4269–4287, 1996.

Crutzen, P. J. and Andreae, M. O.: Biomass burning in the tropics: Impact on atmospheric chemistry and biogeochemical cycles, Science, 250, 1669–1678, 1990.

Crutzen, P J. and Carmichael, G. R.: Modeling the influence of fires on atmospheric chemistry, in: Fire in the Environment: The Ecological, Atmospheric, and Climatic Importance of Vegetation Fires, (Eds) Crutzen, P. J. and Goldammer, J. G., John Wiley, New York, pp. 89–106, 1993.

de Laat, A. T. J., Zachariasse, M., Roelofs, G. J., van Velthoven, P., Dickerson, R. R., Rhoads, K. P., Oltmans, S. J., and Lelieveld, J.: Tropospheric O$_3$ distribution over the Indian Ocean during

spring 1995 evaluated with a chemistry-climate model, J. Geophys. Res., 104, 13 881–13 893, 1999.

de Laat, A. T. J. and Lelieveld, J.: The diurnal O_3 cycle in the tropical and subtropical marine boundary layer, J. Geophys. Res., 105, 11 547–11 559, 2000.

de Laat, A. T. J, Dickerson, R. R., Lelieveld, J., Lobert, J., and Roelofs, G. J.: Source analysis of Carbon MoNO$_X$ide pollution during INDOEX, J. Geophys. Res., D22, 28 481–28 496, 2001.

de Laat, A. T. J. and Lelieveld, J.: Reply, J. Geophys. Res., 104, 1369–1371, 2001.

de Laat, A. T. J. and Lelieveld, J.: Interannual variability of the Indian winter monsoon circulation and consequences for pollution levels over the Indian Ocean, J. Geophys. Res., in press, 2002.

Folkins, I., Loewenstein, M., Podolske, J., Oltmans, S., and Proffitt, M.: A barrier to vertical mixing at 14 km in the tropics: Evidence from ozonesondes and aircraft measurements, J. Geophys. Res., 104, 22 095–22 102, 1999.

Galanter, M., Levy, II, H., and Carmichael, G. R.: Impacts of biomass burning on tropospheric CO, NO$_X$ and O_3, J. Geophys. Res., 105, 6633–6653, 2000.

Ganzeveld, L. N. and Lelieveld, J.: Dry deposition parameterization in a chemistry – general circulation model and its influence on the distribution of chemically reactive trace gases, J. Geophys. Res., 100, 20 999–21 012, 1995.

Ganzeveld, L. N., Lelieveld, J., and Roelofs, G. J.: A dry deposition parameterization for sulfur oxides in a chemistry and general circulation model, J. Geophys. Res., 103, 5679–5694, 1998.

Graedel, T. E. and Crutzen, P.: Atmospheric change: An earth perspective, AT&T, pp. 446, Chapter 8, 1993.

Hao, W. M. and Liu, M. H.: Spatial and temporal distribution of tropical biomass burning, Global Biogeochem. Cycles, 8, 495–503, 1994.

Haskins, R. D., Barnett, T. P., Tyree, M. M., and Roeckner, E.: Comparison of cloud fields from an atmospheric general circulation model, in situ and satellite measurements, J. Geophys. Res., 100, 1367–1378, 1995.

Hastenrath, S.: Climate and circulation in the tropics, Kluwer Academic Press, pp. 455, 1988.

Hertel, O., Berkowicz, R., Christensen, J., and Hov, O.: Test of two numerical schemes for use in atmospheric transport-chemistry models, Atmos. Env. 27A, 2591–2611, 1993.

Hoerling, M. P., Schaack, T. K., and Lenzen, A. J.: A global analysis of stratospheric tropospheric exchange during northern winter, Mon. Wea. Rev., 121, 162–172, 1993.

Jeuken, A. B. M., Siegmund, P.C., Heijboer, L. C., Feichter, J., and Bengtson, L.: On the potential of assimilating meteorological analysis in a climate model for the purpose of model validation, J. Geophys. Res., 101, 16 939–16 950, 1996.

Kentarchos, A. S., Roelofs, G. J., and Lelieveld, J.: Model study of a stratospheric intrusion event at lower midlatitudes associated with the development of a cutoff low, J. Geophys. Res., 104, 1717–1727, 1999.

Kentarchos, A. S., Roelofs, G. J., and Lelieveld, J.: Simulation of extratropical synoptic scale stratosphere-troposphere exchange using a coupled chemistry-GCM: Sensitivity to horizontal resolution, J. Atmos. Sci, 57, 2824–2838, 2000.

Kentarchos, A. J., Roelofs, G. J., and Lelieveld, J.: Altitude distribution of tropospheric ozone over the northern hemisphere during 1996, simulated with a chemistry-GCM at 2 different hori-

zontal resolutions, J. Geophys. Res., 106, 17 543–17 470, 2001.

Lal, S., Naja, M., and Jayaraman, A.: Ozone in the marine boundary layer over the tropical Indian Ocean, J. Geophys. Res., 55, 18 907–18 917, 1998.

Lawrence, M. G. and Lal, S.: Elevated mixing ratios of surface ozone over the Arabian Sea, Geophys. Res. Lett., 28, 1487–1490, 2001.

Lelieveld, J. and van Dorland, R.: Ozone chemistry changes in the troposphere and consequent radiative forcing of climate, in: Atmospheric ozone as a climate gas, (Eds) Wang, W. C. and Isaksen, I. S. A., Springer-Verlag, Berlin, pp. 227–258, 1995.

Leon, J.-F., Chazette, P., Dulac, F., Pelon, J., Flamant, C., Bonazzola, M., Foret, G., Alfaro, S. C., Cachier, H., Cautenet, S., Hamonou, E., Gaudichet, A., Gomes, L., Rajot, J.-L., Lavenu, F., Inmdar, S. R., Sarode, P. R., and Kadadevarmath, J. S.: Large-scale advection of continental aerosols during INDOEX, J. Geophys. Res, 106, 28 427–28 439, 2001.

Mandal, T. K., Kley, D., Smit, H. G. J., Srivastav, S. K., Peshin, S. K., and Mitra, A. P.: Vertical distribution of ozone over the Indian Ocean (15 N–15 S) during the First Field Phase INDOEX 1998, Current Science, 76, 938–943, 1999.

Peshin, S. K., Mandal, T. K., Smit, H. G. J., Srivastav, S. K., and Mitra, A. P.: Observations of vertical distribution of tropospheric ozone over the Indian Ocean and its comparison with continental profiles during INDOEX-FFP-1998 and IFP 1999, Current Science, 80, 197–208, 2001.

Pickering, K. E., Thompson, A. M., Scala, J. R., Tao, W.-K., Dickerson, R. R., and Simpson, J.: Free tropospheric ozone production following entrainment of urban plumes into deep convection, J. Geophys. Res., 97, 17 895–18 000, 1992.

Price, C. and Rind, D.: A simple lightning parameterization for calculating global lightning distributions, J. Geophys. Res., 97, 9919–9933, 1992.

Randriambelo, T., Baray, J. L., Baldy, S., and Bremaud, P.: A Case study of extreme tropospheric ozone contamination in the tropics using in situ, satellite and meteorological data, Geophys. Res. Lett., 26, 1287–1290, 1999.

Rasch, P. J. and Williamson, D.: Computational aspects of moisture transport in global models of the atmosphere. Q. J. R. Meteorol. Soc., 116, 1071–1090, 1990.

Reiner, T., Sprung, D., Jost, D., Gabriel, R., Mayol-Bracero, O. L., Andreae, M. O., Campos, T. L., and Shetter, R. E.: Chemical characterization of pollution layers over the tropical Indian Ocean: Signatures of emissions from biomass and fossil fuel burning, J. Geophys. Res., 106, 28 497–28 510, 2001.

Rhoads, K. P., Kelley, P., Dickerson, R. R., Carsey, T. P., Farmer, M., Savoie, L., and Prospero, J. M.: Composition of the troposphere of the Indian Ocean during the monsoonal transition, J. Geophys. Res., 102, 18 981–18 995, 1997.

Roeckner, E., Arpe, K., Bengtsson, L., Christoph, M., Claussen, M., Dmenil, L., Esch, M., Giorgetta, M., Schlese, U., and Schulzweida, U.: The atmospheric general circulation model ECHAM-4: Model description and simulation of present-day climate, Rep. 218, Max-Planck-Institute for Meteorology, Hamburg, Germany, 1996.

Roelofs, G. J. and Lelieveld, J.: Distribution and budget of O_3 in the troposphere calculated with a chemistry – general circulation model, J. Geophys. Res., 100, 20 983–20 998, 1995.

Roelofs, G. J. and Lelieveld, J.: Model study of the influence of

cross-tropopause O$_3$ transports on tropospheric O$_3$ levels, Tellus, 49B, 38–55, 1997.

Roelofs, G. J., Lelieveld, J., Smit, H. G. J., and Kley, D.: Ozone production and transports in the tropical Atlantic region during the biomass burning season, J. Geophys. Res., 102, 10 637–10 651, 1997a.

Roelofs, G. J., Lelieveld, J., and van Dorland, R.: A three-dimensional chemistry/general circulation model simulation of anthropogenically derived ozone in the troposphere and its radiative climate forcing, J. Geophys. Res., 102, 23 389–23 401, 1997b.

Roelofs, G. J. and Lelieveld, J.: Tropospheric ozone simulated with a chemistry-general circulation model: Influence of higher hydrocarbon chemistry, J. Geophys. Res., 105, 22 697–22 712, 2000.

Siegmund, P. C., van Velthoven, P. F. J., and Kelder, H.: Cross-tropopause transport in the extratroipcal northern winter hemisphere, diagnosed from high-resolution ECMWF data, W. J. R. Meteorol. Soc., 122, 1921–1941, 1996.

Smit, H. G. J., Sträter, W., Kley, D., and Profitt, M. H.: The evaluation of ECC-ozone sondes under quasi flight conditions in the environmental simulation chamber at Jülich, in: Proceedings of Eurotrac Symposium 1994, (Eds) Borell, P. M., et al., SPB Acad., The Hague, the Netherlands, pp. 349–353, 1994.

Smit, H. G. J., Gilge, S., and Kley, D.: JOSIE: The 1996 WMO international intercomparison of ozone sondes under quasi flight conditions in the environmental simulation chamber at Jülich, Tech Doc. 296, World Meteorol. Org., Geneva, 1998.

Thompson, A. M., Pickering, K. E., McNamara, D. P., Schoeberl, M. R., Hudson, R. D., Kim, J. H., Browell, E. V., Kirchhoff, V. W. J. H., and Nganga, D.: Where did tropospheric zone over southern Africa and the tropical Atlantic come from in October 1992? Insights from TOMS, GTE TRACE A and SAFARI 1992, J. Geophys. Res., 101, 24 251–24 278, 1996.

Tiedtke, M.: A comprehensive mass flux scheme for cumulus parameterization in large-scale models, Mon. Wea. Rev., 117, 1779–1800, 1989.

Yienger, J. J. and Levy, II, H.: Empirical model of global soil-biogenic NO$_X$ emissions, J. Geophys. Res., 100, 11 447–11 464, 1995.

Zachariasse, M., van Velthoven, O. F. J., Smit, H. G. J., Lelieveld, J., Mandal, T. K., and Kelder, H.: Influence of stratosphere-troposphere exchange on tropospheric ozone over the tropical Indian Ocean during the winter monsoon, J. Geophys. Res., 105, 15 403–15 416, 2000.

Zachariasse, M., Smit, H. G. J., van Velthoven, P. F. J., and Kelder, H.: Cross-troposphere and interhemispheric transports into the tropical free troposphere over the Indian Ocean, J. Geophys. Res., 106, 28 441–28 453, 2001.